RSC Advances

PAPER

View Article Online
View Journal | View Issue

Cite this: *RSC Adv.*, 2022, **12**, 3062

Preparation and characterization of three-dimensional hierarchical porous carbon from low-rank coal by hydrothermal carbonization for efficient iodine removal

Yufeng Yin,[a] Dingcheng Liang,*[a] Deqian Liu[a] and Qianjun Liu[b]

Low-rank coal, such as Shengli lignite (SL) and Datong bitumite (DT), has abundant reserves and is low in cost. Due to its high moisture content, abundant oxygen-containing groups, high ash content and low calorific value, low-rank coal is mainly used in a low-cost method of direct combustion. For better value-added utilization of SL and DT, a novel strategy has been developed for the preparation of oxygen-rich hierarchical porous carbons (HPCs) by hydrothermal carbonization (HTC), followed by steam activation. In this paper, firstly, the physical and chemical properties of SL and DT were improved by HTC pretreatment, bringing them closer to high rank coal. Then, the effects of HTC pretreatment and activation temperature on the properties of the HPCs were investigated in detail. The results show that the HPCs have mainly microporous structures (the microporosity of 200-SLHPC-900 is 79.58%) based on the N_2 adsorption–desorption isotherm analysis and exhibit a higher specific surface area (SSA) and larger pore volume (25.02% and 2.69% improvement for 200-SLHPC-900; 4.93% and 14.25% increase for 200-DTHPC-900, respectively) after HTC pretreatment. The two types of HPCs also present good adsorption performance. The iodine adsorption value of lignite-based HPC presents an increase of 13.72% from 503 mg g^{-1} to 572 mg g^{-1}, while the value of bitumite-based HPC increases up to 924 mg g^{-1}. A preliminary additional HTC step is therefore an effective method by which to promote the performance of low-rank coal based porous carbon. The process of hydrothermal carbonization and steam activation is a cost-effective and environmentally-friendly preparation method, which omits the use of a chemical activator and reduces the step of alkaline waste liquid discharge compared with the route of carbonization and chemical activation.

Received 3rd November 2021
Accepted 9th January 2022

DOI: 10.1039/d1ra08016d

rsc.li/rsc-advances

1. Introduction

Iodine-containing wastewater produced in the pharmaceutical industries, nuclear power plants and disinfection process of iodophor can result in a series of serious problems, such as contaminating underground water sources and threatening the life of creatures due to its toxicity.[1–4] Therefore, iodine removal from wastewater is an urgent problem to be solved globally and it is of great importance to improve civil health and boost the sustainable development of the environment. Multiple methods, such as membrane separation, chemical reaction binding and adsorption, have been proposed and applied for the removal of iodine.[5,6] Of these methods, adsorption has become one of the most attractive wastewater treatment technologies because of its high efficiency, simple operation and low cost. Specifically, porous carbons (PCs) have higher chemical and structural stabilities compared with metal–organic frameworks and nanoporous organic polymer networks,[7,8] and have been primarily prepared from biomass wastes,[9] coal,[10] pitch,[11] petroleum and their derived products[11] *via* template-based, chemical activation or physical activation methods.[12,13] Of a variety of raw materials, coal is still the main material used to produce PCs due to its easy availability, low cost and high carbon content.

Coal is the primary energy resource in China,[14] and the country has abundant reserves, especially of low-rank coal, of around 200 billion tons, such as Shengli lignite from Inner Mongolia and Datong low metamorphism bitumite from Shanxi, China. Unfortunately, the energy density of low-rank coal is lower than that of anthracite coal due to its higher inherent moisture, oxygen content, ash content and lower carbon content, which limits its application in combustion and gasification.[15] Nonetheless, the high reactivity and oxygen-containing functional groups content of low-rank coal have attracted increased attention towards its use as a precursor for porous carbon.[16,17]

[a]*School of Chemical and Environmental Engineering, China University of Mining & Technology (Beijing), Beijing, 100083, China. E-mail: liangdc@cumtb.edu.cn*
[b]*Department of Petroleum and Geosystems Engineering, The University of Texas at Austin, Austin, TX, 78712, USA*

In the past 10 years, hydrothermal carbonization (HTC) has attracted increasing interest in the field of materials science engineering, as it can be used to synthesize functional carbon materials.[18] HTC products feature abundant oxygen-containing functional groups, thus making them suitable for many applications, such as adsorption, drug delivery, catalyst supports and the synthesis of porous carbon.[19,20] Moreover, the presence of oxygen-containing species in the precursor increases the number of activable sites, thus leading to an increase in the porosity of PCs.[21] Simultaneously, the obtained hydrochar can be easily modified, allowing the introduction of heteroatoms such as N, S, P, and Fe, besides O, which is conducive to different functionalized products being obtainable.[22] The process of producing synthetic coal from biomass at low temperatures has been known for more than 100 years and has recently regained greater attention in the synthesis of functional carbon materials because of its crucial applications in adsorption, energy storage, separation science, catalysis, and biomedicine, among others.[23,24] Furthermore, hydrothermal pretreatment is a mild, green and environmentally-friendly carbonization technology, as the reactions are carried out in enclosed system conditions at relatively low carbonization temperatures. Recently, several researchers synthesized PCs, carbon spheres, carbon nanotubes, carbon quantum dots and graphene *via* the hydrothermal treatment of biomass.[25,26] For instance, Hao *et al.*[27] used waste sugar solution to prepare porous carbon spheres with a high specific surface area of up to 2293 $m^2\ g^{-1}$ and good electrochemical performance for supercapacitors. Falco *et al.*[23] prepared activated carbon successfully from lignocellulosic biomass *via* HTC and its chemical activated form shows high performance in CO_2 capture and high-pressure CH_4 storage. It is well-known that low-rank coals are not suitable as coking raw materials and are frequently carbonized and upgraded *via* HTC treatment. However, PCs derived from low-rank coal *via* HTC pretreatment and applied in the field of adsorption are rarely reported.

In this paper, lignite and bitumite were selected as raw materials to prepare three-dimensional HPCs *via* hydrothermal carbonization and steam activation. Firstly, the two low-rank coals were pretreated by HTC in a Teflon-lined autoclave and the as-obtained hydrochar was activated by steam. Besides this, the effects of HTC pretreatment and activation temperature on the pore structure properties, the surface chemistry and adsorption performance of the coal samples were investigated. The results achieved in this study not only have certain industrial reference significance for HPCs for the removal of iodine from wastewater, but also help to improve the high value-added utilization of two types of low-rank coal.

2. Experimental

2.1. Raw materials

Shengli lignite (SL) from Inner Mongolia and Datong bitumite (DT), which was collected from Shanxi, China, were used as the raw materials in this study. The proximate and ultimate analyses of SL and DT are listed in Table 1. Reagent grade chemicals were used in all of the experiments. Iodine and potassium iodide were provided by Xilong Chemical Co. Ltd. Sodium thiosulfate, hydrochloric acid and starch were purchased from Tianjin Chemical Reagent Research Institute Co. Ltd.

2.2. Preparation of the HPCs

The HPCs were prepared *via* a two-stage process involving HTC and steam activation. Step 1, 15.0 g of low-rank coal (SL and DT) and 100 mL of deionized water were added to 200 mL Teflon-lined autoclaves, which were then heated at a preset temperature of 200 °C for 8 h. After the autoclave was allowed to cool to room temperature, the resultant product was filtered and washed with deionized water more than three times, followed by desiccation at 110 °C for 24 h. The obtained hydrothermal products were named 200-SLhydrochar and 200-DThydrochar, where 200 represents the HTC temperature. For comparison, SLchar-600 was obtained *via* direct pyrolysis at 600 °C for 30 min under a N_2 atmosphere.

Step 2, the hydrochar was filled into a home-made mold and extruded into a cake block with a diameter of 25 mm and a thickness of 8 mm under a pressure of 200 MPa. After natural air drying, the block was broken into granular material with a particle size of 3–10 mm. The hydrochar was then activated by steam (0.8 mL $g_{hydrochar}^{-1}\ h^{-1}$) produced from a steam generator in a horizontal tube furnace at a heating rate of 10 °C min^{-1} up to the final temperatures (900, 950 and 1000 °C) and held for 3 h under a N_2 atmosphere. After cooling, the activated samples were dried at 150 °C under vacuum for 2 h. The obtained HPCs were denoted as 200-DTHPC-900 (200 represents the HTC temperature and 900 is the activation temperature) and 200-SLHPC-*y* (200 represents the HTC temperature and *y* is 900, 950, and 1000, representing the activation temperature). For comparison, SL and DT were also individually activated by the same steam flux at 900 °C for 3 h without hydrothermal carbonization pretreatment and were designated as SLPC-900 and DTPC-900. Besides this, the graphical schematic for the preparation of HPCs is illustrated in Fig. 1.

2.3. Sample characterization

All samples to be characterized were pulverized through 200 mesh and dried at 110 °C for 24 h. X-ray diffraction (XRD) measurements were performed on a Bruker D8 Advance diffractometer using Cu Kα radiation operated at 40 mA and 40 kV (10° min^{-1} from 10 to 90°). Raman analysis of the hydrochar and HPC samples was carried out on a Bruker Senterra Raman spectrometer by 532 nm laser excitation using a microscope. The Raman spectra were obtained in the range of 1000–2000 cm^{-1}, and all scans were performed three times. Field-emission scanning electron microscopy (FESEM) images were measured using a Merlin Zeiss microscope operated at 5.0 kV to observe the morphology of the samples. The surface chemical properties of the samples were characterized qualitatively using a Nicolet Magna IR560 Fourier-transform infrared (FTIR) spectrometer. X-ray photoelectron spectroscopy (XPS) data were collected using a Thermo ESCALAB 250Xi spectrometer to analyze the surface oxygen-containing functional groups. N_2 adsorption–desorption isotherms were measured at −196 °C

Table 1 Proximate and ultimate analysis of two low-rank coals before and after hydrothermal carbonization[a]

	Proximate analysis (wt%)				Ultimate analysis (wt%)						
Sample	M_{ad}	A_d	V_{daf}	FC_{daf}[b]	C_{daf}	H_{daf}	O_{daf}[b]	N_{daf}	S_{daf}	$A_{O/C}$	$A_{H/C}$
SL	13.41	14.48	45.59	54.41	66.15	4.30	25.88	1.21	2.46	0.391	0.065
200-SLhydrochar	8.43	12.44	43.48	56.52	70.20	3.62	23.60	1.12	1.46	0.336	0.052
DT	6.97	4.34	33.36	66.64	76.65	7.10	14.11	1.13	1.01	0.184	0.093
200-DThydrochar	5.83	4.01	32.31	67.69	78.04	6.45	13.75	1.05	0.71	0.176	0.083

[a] Note, ad: air dry basis; d: dry basis; daf: dry ash-free. [b] By difference.

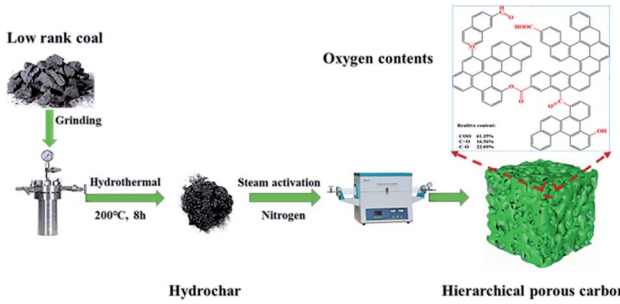

Fig. 1 Graphical schematic of the preparation of the HPCs.

using a Quantachrome Autosorb-iQ instrument. The SSA was obtained using the Brunauer–Emmett–Teller (BET) method. Micropore surface area and micropore volume were calculated using the *t*-plot method. The total pore volume was determined at a relative pressure, P/P_0, of 0.99. The pore size distribution was calculated from the N_2 adsorption data using density functional theory (DFT).

2.4. Adsorption experiments

HPCs was selected as adsorbents to evaluate the adsorption performance of iodine (I_2). The I_2 adsorption tests were carried out following the ASTM D4607-86 method. Dried HPCs were weighed and then added to 250 mL flasks containing 10 mL of 5 wt% HCl solution. The flasks were then gently swirled until the HPCs were completely wetted; 100 mL of 0.1 N I_2 solution was added to the flasks and then they were strongly shaken for 30 s before the products were filtered. A standardized 0.1 N sodium thiosulfate solution was used to titrate the filtered solutions using starch indicator. The I_2 adsorption value Q (mg g^{-1}) on the HPCs was calculated based on the following equation:

$$Q = \left(C_1V_1 - \frac{V_1 + V_2}{V}C_2V_3\right)\frac{M}{m}$$

where C_1 and C_2 (mol L^{-1}) are the concentrations of I_2 and sodium thiosulfate solutions, respectively, and V_1, V_2 and V_3 (mL) are the consumed volumes of I_2, hydrochloric acid and sodium thiosulfate solution, respectively. V (mL), M (126.9 mg g^{-1}) and m (g) represent the volumes of filtrate, half the molecular weight of I_2 and the weight of porous carbon, respectively.

3. Results and discussion

3.1. Structural characterization of hydrochar and porous carbon samples

3.1.1. Proximate and ultimate analysis. Proximate and ultimate analysis results of SL and DT before and after HTC treatment are shown in Table 1. The M_{ad} (moisture content of air dry base) content of SL presents a significant decrease after HTC pretreatment from 13.41 wt% to 8.43 wt%. This result confirms that inherent moisture is removed irreversibly and that the water-holding capacity of coal decreases after HTC treatment. The volatile content of SL decreased down to 43.48 wt%, while its fixed carbon increased up to 56.52 wt%. These results clearly show that HTC boosts lignite carbonization and volatile matter decomposition, thereby resulting in an enhancement in the properties of lignite. Another type of low-rank bituminous coal, DT, shows same trends in lower M_{ad} content, less volatile content and more fixed carbon content after HTC treatment.

Ultimate analysis of SL and DT shows that carbon content increased, whereas the oxygen content decreased significantly after the HTC process. Decreases in the atomic ratios of oxygen to carbon ($A_{O/C}$) and hydrogen to carbon ($A_{H/C}$), which are related to coal rank, indicate partial removal of oxygen-containing functional groups and an improvement in properties in terms of coal rank. Furthermore, the losses in oxygen are related to the dehydration, decarboxylation and reduction reactions.[28]

In summary, it is worth noting that low-rank coals after HTC modification might be considered to be somewhat similar to higher-rank coals, and that HTC can be regarded as somewhat analogous to the coalification process, which can be greatly accelerated by the application of temperature and pressure.

3.1.2. XRD analysis. The microcrystalline structures of the samples were measured by XRD. The XRD patterns of SL and DT before and after HTC treatment are shown in Fig. 2(a) and (b). The XRD patterns of the two low-rank coals present two typical diffraction peaks at $2\theta = 24°$ and 43°, which correspond to the (002) and (100) crystal planes of graphite, respectively, revealing the great graphitization degree of 200-SLhydrochar and 200-DThydrochar.[29] It is of interest to note that the intensities of the diffraction peaks at 24° and 43° slightly decrease and the peaks exhibit weak broadening, illustrating a slight increase in the graphitization degree and the formation of an amorphous carbon phase after HTC. Furthermore, the DT shows a similar

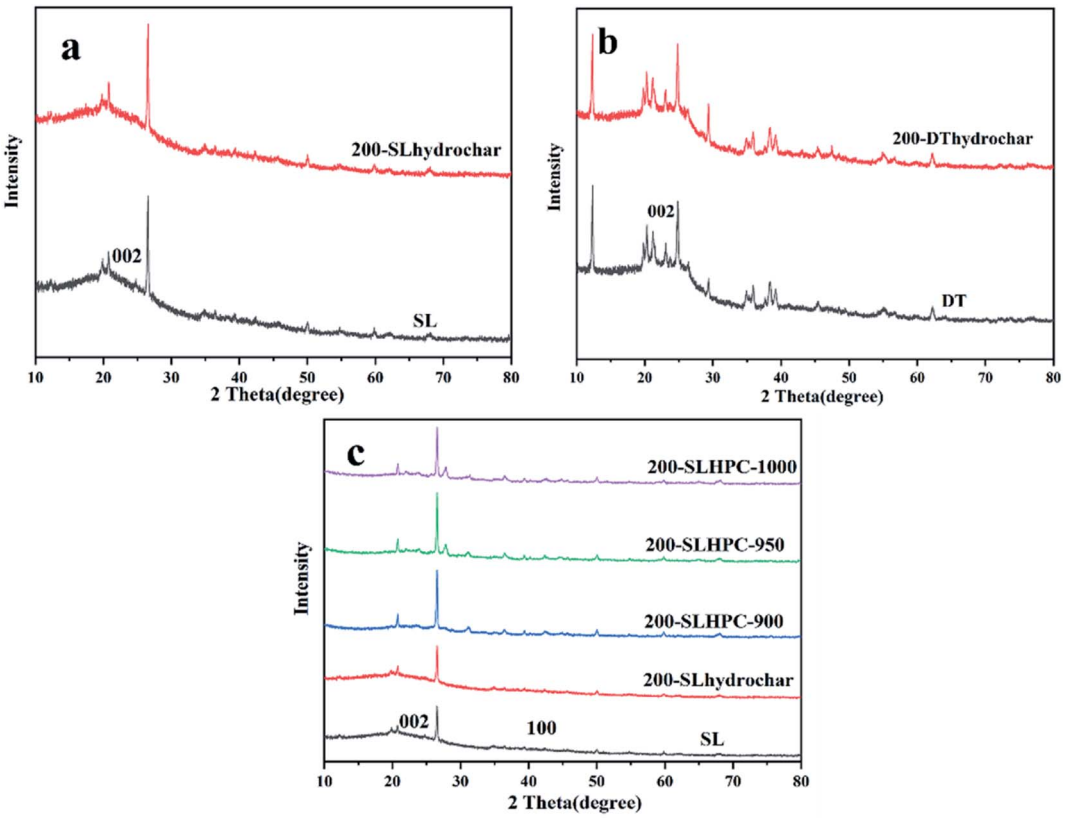

Fig. 2 XRD patterns of (a) SL and 200-SLhydrochar; (b) DT and 200-DThydrochar; (c) SL and 200-SLHPC-*y* at different activation temperatures.

trend to that of the SL after HTC pretreatment. As shown in Fig. 2(c), the peak at 24° (002) became weak and almost vanished upon an increase in the activation temperature, revealing that high temperature destroys the graphitic crystalline structures of the samples upon activation and etching.[30]

3.1.3. Raman spectroscopy analysis. Raman spectroscopy is a powerful tool that is used to investigate the degree of crystallinity, defects, and disorder in carbon materials.[31] Thus, it was used to characterize the structural evolution of the SLhydrochar and SLHPC samples derived from SL lignite under hydrothermal carbonization and steam activation conditions to determine the optimal preparation conditions to prepare hierarchical PCs with rich porosity and a mainly amorphous carbon structure. The Raman spectra of the samples are shown in Fig. 3(a). The D-band represents the defective and disordered structure of the char samples. The G-band is related to the in-plane vibrations of sp^2 carbon in a hexagonal lattice. The amorphous degree of a sample can be appraised based on the intensity ratio of I_D/I_G (I_D and I_G are the intensities of D- and G-bands, respectively).[32] As shown in Fig. 3(b), the I_D/I_G values of SL, 200-SLhydrochar and SLchar-600 are 0.42, 0.53 and 0.62, respectively. A slight increase in intensity ratio is observed with an increase in the carbonization temperature, which is related to the formation of polycyclic aromatic units *via* the condensation of the macromolecular network in the char. During this stage, the chemical bonds between the macromolecular compounds were broken to form micromolecules. These micromolecules deposited on the surface of the char, which resulted in the formation of a lot of defects. Nevertheless, the I_D/I_G increased to 1.06 after activation of the samples. This indicates that the structure of 200-SLHPC-1000 has more defects than the other samples, which might be because its crystalline structure is destroyed by more severe steam activation at a temperature of 1000 °C.

3.1.4. FESEM analysis. The micromorphologies of the samples were also observed by FESEM, with the images presenting significant differences under different conditions, as shown in Fig. 4. It can be seen from Fig. 4(a) and (b) that 200-SLhydrochar exhibits the smoothest surface, fewer particles and a more pronounced outline compared with the other samples, while the surface of SL lignite is filled with a large number of fine and irregular particles that are loose and do not have clear external contours. This indicates that the micromolecules of organic matter cracked, and were then processed through a condensation polymerization reaction into polycyclic aromatic hydrocarbons.[16] Furthermore, the prepared activated samples reveal a typical three-dimensional structure, where, peculiarly, 200-SLHPC-900 (Fig. 4(c) and (d)) exhibits a hierarchical PC structure with a pore size distribution made up of a combination of different pore types (macropores, mesopores and abundant micropores) after etching with an excess of steam. The three-dimensional hierarchical porous structure of the sample features a large number of active sites for subsequent adsorption. In addition, the prepared HPC indeed shows well-developed porosity in its microcrystalline and amorphous

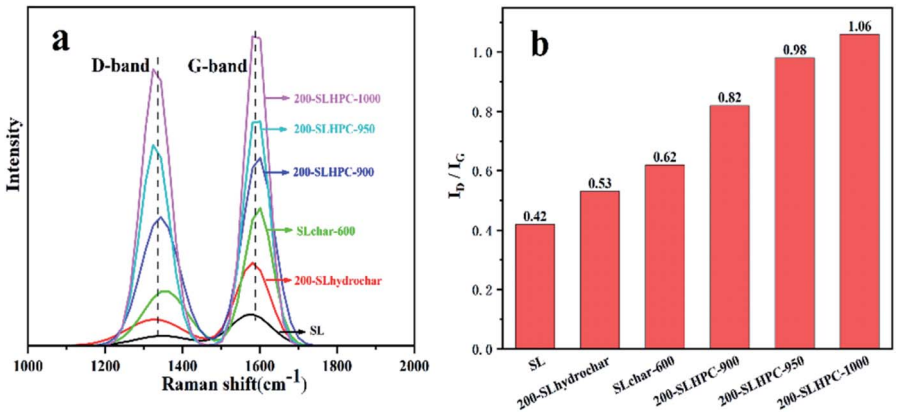

Fig. 3 (a) Raman spectra and (b) I_D/I_G intensity ratios of the SL char samples.

structure. As shown in Fig. 4(e) and (f), the special morphology of 200-SLHPC-1000 might be due to the 200-SLhydrochar being etched by steam during its activation at a high temperature (1000 °C), meaning that its original structure is destroyed to form a three-dimensional and flocculent porous structure in the interior of the carbonized samples. Overall, the FESEM results

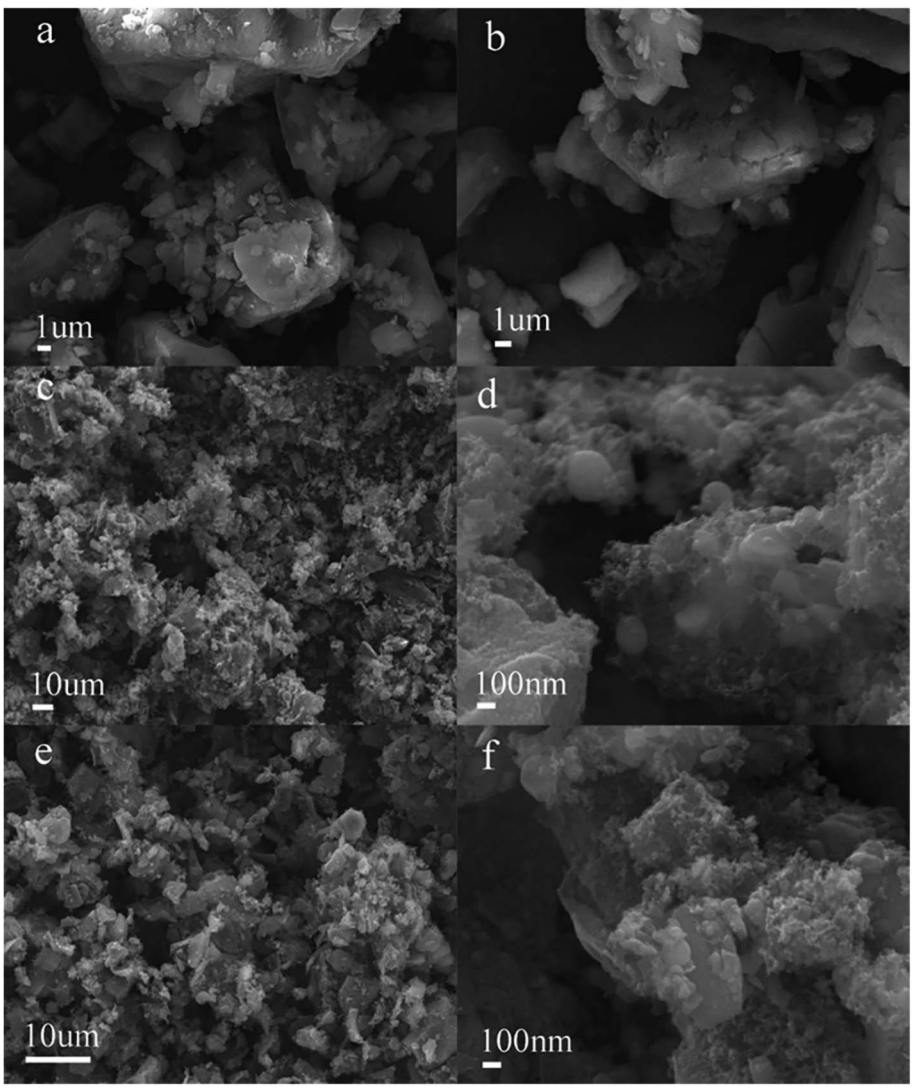

Fig. 4 SEM images of (a) SL, (b) 200-SLhydrochar, (c and d) 200-SLHPC-900 and (e and f) 200-SLHPC-1000.

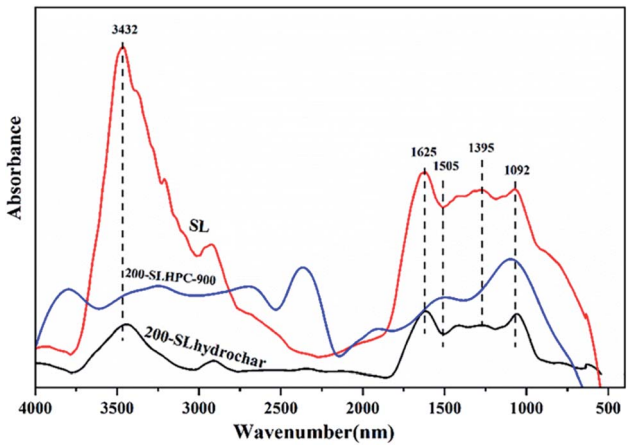

Fig. 5 FTIR spectra of SL, 200-SLhydrochar and 200-SLHPC-900.

prove the effects that steam activation has on the pore structure development of HPC from hydrochar.

3.2. Surface chemistry characterization of the hydrochar and porous carbon samples

3.2.1. FTIR spectroscopy analysis. FTIR spectroscopy was used for the immediate detection of the surface chemical properties of coal, hydrochar and HPCs derived from the different heat treatment processes. As shown in Fig. 5, it is obvious that the oxygen-containing functional groups of 200-SLHPC-900 are different from those of SL and 200-SLhydrochar based on the spectra patterns of 200-SLHPC-900, 200-SLhydrochar and SL over the range of 4000–400 cm^{-1}. From a review of numerous papers, the band at 3432 cm^{-1} can be attributed to –OH stretching.[33] The bands at 1620 cm^{-1} might be due to the stretching vibrations of C=O in carbonyl, ester, or carboxyl groups and 1395 cm^{-1} can be attributed to C–H asymmetrical bending, respectively.[34] The strong bands at around 1350–1000 cm^{-1} represent the stretching vibrations of C=O in hydroxyl, ester, and ether groups and the bending vibration of –OH. The peak at around 783 cm^{-1} may be assigned to the bending of hydrogen in various locations in the aromatic rings and the peak at 990 cm^{-1} can be assigned to C–O.[35] After HTC pretreatment, some oxygen-containing functional groups of 200-SLhydrochar showed significant changes. For instance, the intensities of the –COOH (1620 cm^{-1}) and –OH (3600–3200 cm^{-1}) peaks become weaker, while the intensity of the C=O (1690–1640 cm^{-1}) peaks increase, which can be assigned to the stretching of the conjugated aromatic carbonyl moiety. These phenomena might be caused by intramolecular and intermolecular decarboxylation, dehydration and aromatization during the HTC process.[36] It is also worth noting that some

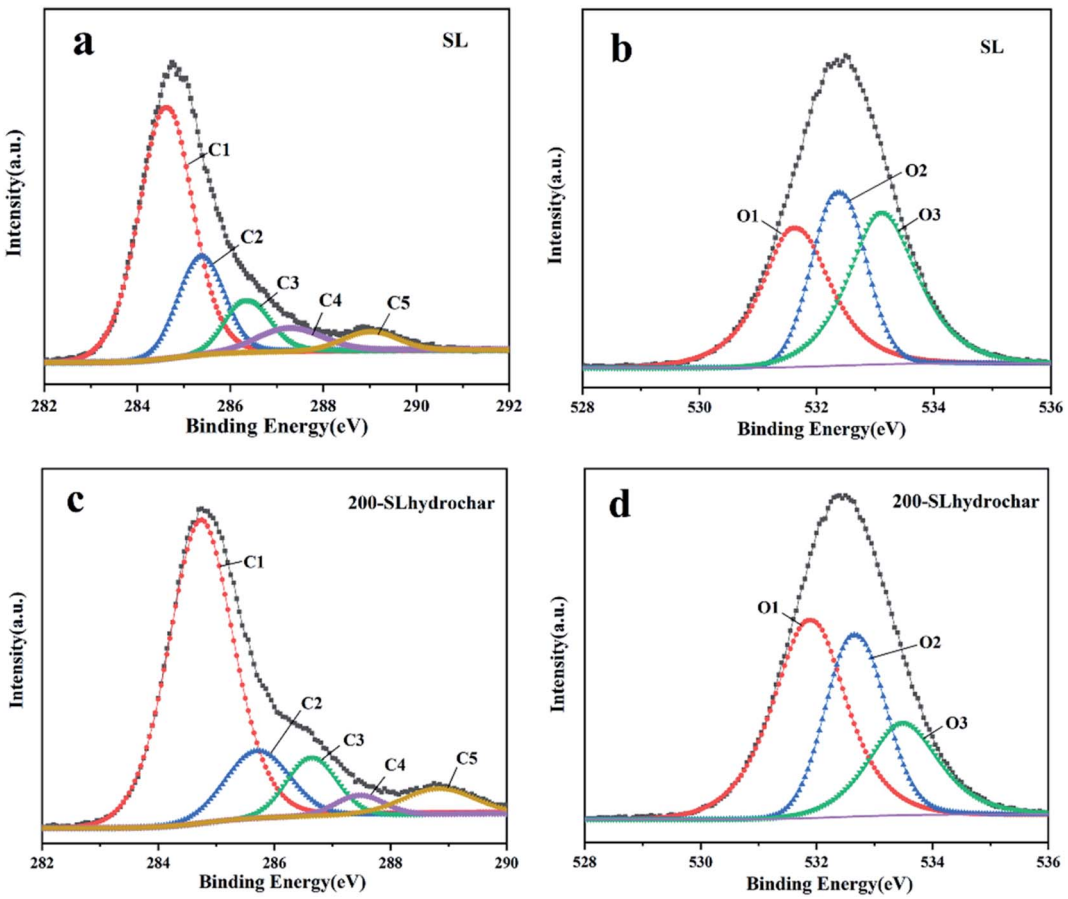

Fig. 6 High-resolution XPS spectra of (a and c) C 1s and (b and d) O 1s of SL and 200-SLhydrochar.

Table 2 Relative contents of the functional groups of SL and 200-SLhydrochar in the XPS spectra

		C 1s					O 1s		
Sample	O/C[a]	C1 (%)	C2 (%)	C3 (%)	C4 (%)	C5 (%)	O1 (%)	O2 (%)	O3 (%)
SL	0.394	56.18	20.22	10.67	7.87	5.06	33.58	29.93	36.50
200-SLhydrochar	0.328	67.11	14.09	9.40	3.36	6.04	46.08	32.72	21.20

[a] Atomic ratio.

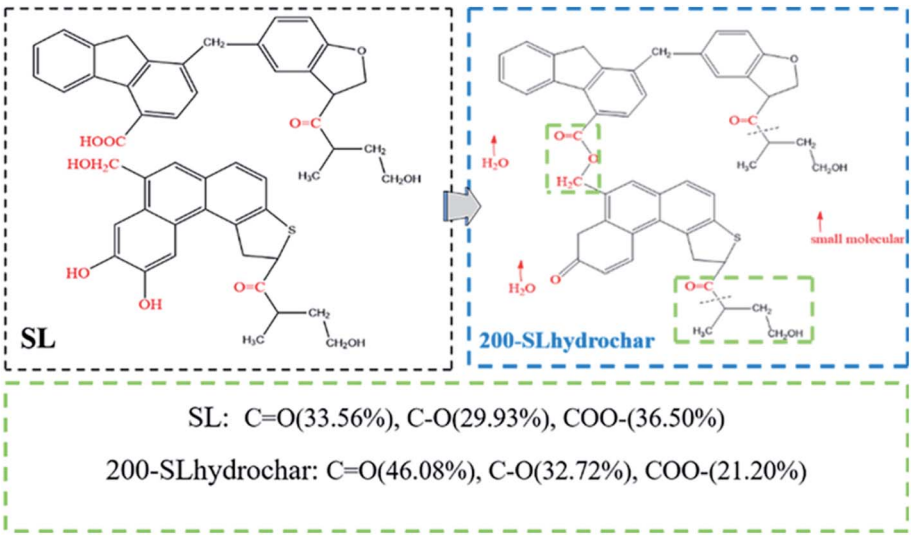

Fig. 7 Evolution of surface functional groups during the hydrothermal carbonization of SL.

peaks can be observed to appear and disappear after steam activation, and the newly increased peak intensities of the functional groups are those of oxygen-containing species, such as the C–O (1300–1100 cm^{-1}) of an ether. This might be due to activation by steam resulting in structural damage to the organic macromolecules of 200-SLhydrochar, thus generating new functional groups. Some scholars have reported that steam works not only as a dehydrating agent but also as an oxidizing agent during the activation process.[37] Furthermore, these oxygen-containing species improve the adsorptive performance of the HPCs *via* improved wettability and the formation of chemisorption active sites.

3.2.2. XPS analysis. To further understand the surface compositions and evolution of chemical states during the hydrothermal carbonization process, SL and 200-SLhydrochar were investigated by XPS. The high-resolution C 1s and O 1s peaks were curve-fitted using the Thermo Avantage software based on relevant literature. As shown in Fig. 6, the fitted peaks of the C 1s XPS spectra are approximately located at 284.7 eV (C1), 285.5 eV (C2), 286.5 eV (C3), 287.6 eV (C4) and 288.4 eV (C5), corresponding to C–C/C=C, C–H, C–OH in hydroxyl or ether groups, C=O in carbonyl groups and O=C–O in carboxylic or ester groups, respectively.[38] The fitted peaks of the O 1s XPS spectra are approximately located at 531.8 eV (O1), 533.1 eV (O2) and 534.2 eV (O3), corresponding to C=O in ester or

Table 3 Pore structure characteristics of PC samples treated with different carbonization methods and activation temperatures

Sample	S_{BET}[a] ($m^2\ g^{-1}$)	V_t[b] ($cm^3\ g^{-1}$)	S_{mic}[c] ($m^2\ g^{-1}$)	S_{mes}[d] ($m^2\ g^{-1}$)	V_{mic}[c] ($cm^3\ g^{-1}$)	V_{mes}[d] ($cm^3\ g^{-1}$)	D_{ave}[e] (nm)
DTPC-900	609.471	0.3396	551.291	58.180	0.246	0.095	2.427
200-DTHPC-900	639.493	0.3880	581.313	58.180	0.246	0.095	2.229
SLPC-900	348.218	0.3537	272.787	75.431	0.143	0.225	4.063
200-SLHPC-900	435.351	0.3806	346.465	88.886	0.168	0.225	3.731
200-SLHPC-950	464.972	0.371	390.413	74.559	0.183	0.198	3.313
200-SLHPC-1000	548.991	0.414	483.170	65.821	0.223	0.199	3.017

[a] S_{BET}: specific surface area from multiple BET method. [b] V_t: total pore volume at $P/P_0 = 0.99$. [c] S_{mic}, V_{mic}: *t*-method micropore surface area and micropore volume. [d] S_{mes}, V_{mes}: difference of S_{BET}, S_{mic}, and V_t, V_{mic}, respectively. [e] D_{ave}: average pore diameter.

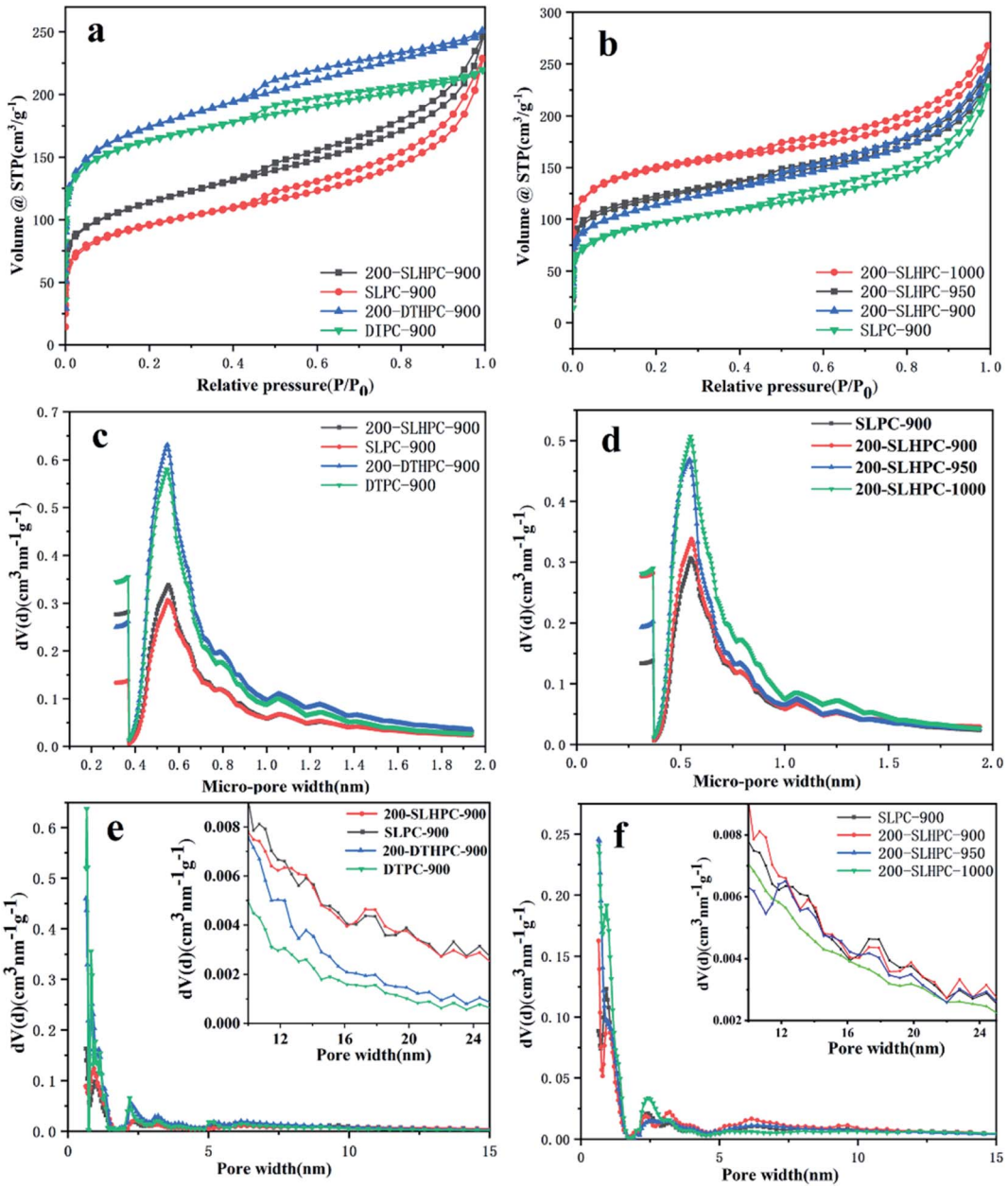

Fig. 8 Nitrogen adsorption–desorption isotherms (a and b), micropore size distribution patterns (c and d) and pore size distribution patterns (e and f) of DTPC-900, 200-DTHPC-900, SLPC-900 and 200-SLHPC-y.

anhydride groups, C–O in hydroxyl groups or ether and COO– in carboxylic groups, respectively.[39]

Furthermore, the XPS results revealed the relative percentage of each component in the SL and 200-SLhydrochar, as shown in Table 2. The species and amounts of oxygen-containing functional groups changed and O/C atomic ratio also reduced from 0.394 to 0.328, based on Table 2 and Fig. 6. The C–OH and –COOH might be transformed to C–O–C and O=C–O, respectively, according to the foregoing analysis of the FTIR spectra. This is most likely due to intramolecular and intermolecular decarboxylation, dehydration, condensation and aromatization during the HTC process. Therefore, the presumed evolution of surface oxygen-containing functional groups during the hydrothermal carbonization of SL is shown in Fig. 7 based on ultimate analysis, FTIR and XPS characterization analysis results.

3.3. Textural properties and adsorption performance of HPCs

The pore structure of porous carbon was investigated by N_2 adsorption–desorption experiments referring to previous reports.[40] The effects of HTC pretreatment and activation temperature on the porous structures of the HPCs are shown in Table 3.

3.3.1. Influence of hydrothermal carbonization pretreatment on porosity and adsorption performance. The nitrogen

adsorption isotherms and corresponding pore size distributions (PSDs) of the four types of PCs are shown in Fig. 8(a), (c) and (e). The isotherms of the PCs show that the curves increase sharply under relatively low pressure and present a slower increase under high pressure (Fig. 8(a)), corresponding to a combination of types I and IV isotherms with an H4 hysteresis loop according to the IUPAC classification, indicating that the pore structures of the PCs include micropores and mesopores, with micropores occupying the greatest percentage. As shown in Table 3, the SSA and total pore volume of 200-SLHPC-900 and 200-DTHPC-900 changed significantly compared with SLPC-900 and DTPC-900. Due to the appropriate HTC temperature (200 °C), 200-SLHPC-900 reaches a larger SSA of 435.351 $m^2\ g^{-1}$ and a bigger pore volume of 0.3806 $cm^3\ g^{-1}$ which is much higher than that of SLPC-900 (348.218 $m^2\ g^{-1}$ and 0.3537 $cm^3\ g^{-1}$, respectively). And 200-DTHPC-900 also has a better SSA of 639.493 $m^2\ g^{-1}$ and pore volume of 0.3880 $cm^3\ g^{-1}$ in comparison to SLPC-900 (SSA of 609.471 $m^2\ g^{-1}$ and pore volume of 0.3396 $cm^3\ g^{-1}$, respectively). The SSA and pore volume of the SL lignite based PC increased by 25.02% and 7.61% times, while those of DT bitumite based PC increased by 4.93% and 14.25% times, respectively. Moreover, the textural properties of the HPCs are better than those of the PCs, owing to the hydrochar having a higher carbon matrix content, larger activable sites and a smaller number of micropores after HTC.[41] After activation by steam, new micropores were formed and the existing pores were enlarged, leading to a promotion in porosity development. The average pore sizes of the two types of coal-based PC after HTC pretreatment decreased from 4.063 to 3.731 nm and 2.427 to 2.229 nm, respectively, and the micropores of the four PCs are mainly concentrated in the vicinity of 0.5 nm, while the mesopores are mainly concentrated in the vicinity of 2.3 nm.

Besides this, the pore development of PCs has also been shown to be reflected by the iodine adsorption value and the loss on ignition (LOI), from a review of many studies.[42,43] The LOI and the iodine adsorption value of the four types of PCs are shown in Fig. 9, from which it can be seen that the two low-rank coal-based PCs with HTC pretreatment have higher iodine adsorption values from the 503 mg g^{-1} of SLPC-900 to the 572 mg g^{-1} of 200-SLHPC-900 and 857 mg g^{-1} of DTPC-900 to 924 mg g^{-1} of 200-DTHPC-900, respectively, indicating that they have enhanced pore structures and good adsorption performance. However, lignite-based PCs have higher LOI values than those of bituminous coal-based PCs, as their degree of metamorphism is relatively low, molecular weight is smaller and their activation reaction is more intense. Furthermore, the higher LOI values of HPCs are due to the partial removal of the side and branched chains of the organic macromolecules during the HTC treatment stage *via* dehydration, decarboxylation and condensation reactions.

3.3.2. Influence of activation temperature on porosity. Compared with the steam flux and activation time, the activation temperature has a more significant impact on the properties of HPCs in the physical activation process. In this part, the HPCs were prepared at activation temperatures of 900, 950 and 1000 °C during the HTC process. As shown in Table 3, the SSA and micropore volume increase by 26.10% and 8.66%, respectively, upon an increase in the activation temperature from 900 to 1000 °C, while the mesoporous SSA presents a slight decreasing trend, indicating that a more intense activation reaction transformed the mesopores into macropores at a higher activation temperature. At the same time, the higher activation temperature not only generates new micropores and increases the microporosity of the SSA, but also further reduces the average pore size from 3.731 nm for 200-SLHPC-900 to 3.017 nm for 200-SLHPC-1000. Fig. 8(d) and (f) show that the pore size distribution of 200-SLHPC-1000 mainly ranges from 0.6 to 4.5 nm, and that it has the greatest number of pores among the four HPCs. At a pore size of greater than 4.5 nm the quantity of pores is the lowest, which may be due to a reduction in mesopores and macropores caused by the burning-off and collapse of the pore wall.[44] The nitrogen adsorption isotherm of 200-SLHPC-1000 is shown in the Fig. 8(b), wherein the curve presents a sharper increase under a low relative pressure of less than 0.2 and a smaller hysteresis loop under high relative pressure, indicating that its pore structure features a larger proportion of micropores and fewer mesopores compared with 200-SLHPC-900.

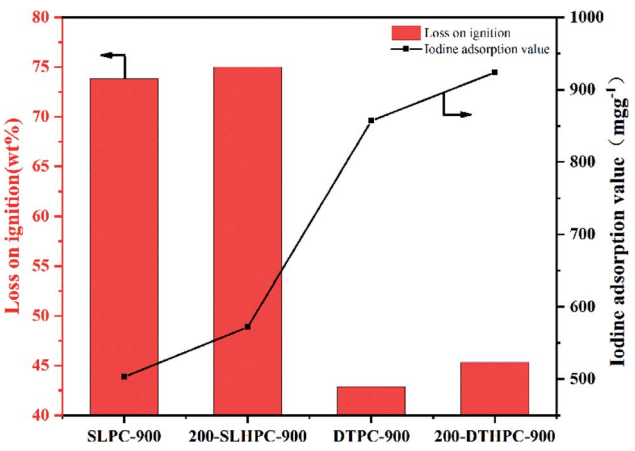

Fig. 9 LOI and iodine adsorption values of the four types of PCs.

4. Conclusion

Lignite and bitumite have been obviously modified, upgraded, and found to be more inclined to have the physicochemical properties of high-rank coals after hydrothermal carbonization, which promotes subsequent steam activation due to the samples featuring more carbon matrix content and active sites. And the two low-rank coals pretreated using the HTC process are attractive precursors for the preparation of three-dimensional structural HPCs with abundant oxygen-containing species *via* steam activation. The procured HPCs present a better hierarchical pore structure and excellent adsorption performance in comparison to materials prepared *via* the normal preparation process in the absence of HTC pretreatment. 200-SLHPC-900 exhibits a better iodine adsorption value of 572 mg g^{-1} compared with the 503 mg g^{-1}

observed for SLPC-900, while this figure for 200-DTHPC-900 increased by 7.82%, from 857 to 924 mg g^{-1}. This is mainly due to the SSA and pore volume of 200-SLHPC-900 increasing by 25.02% and 2.69% and those of 200-DTHPC-900 increasing by 4.93% and 14.25%, respectively. Meanwhile, the hierarchical porous structure development and pore size distribution could be controlled by the activation temperature. Hence, this mild and novel strategy could not only be used to prepare promising coal-based PCs for use as adsorption materials with good performance but also for achieving environmentally-friendly and high value-added applications using low-rank coal. Future work will focus on exploring the reaction mechanism of the HTC of low-rank coal with the addition of a catalyst.

Author contributions

Yufeng Yin: conceptualization, data curation, formal analysis, investigation, methodology, project administration, resources, writing – original draft, writing – review & editing. Dingcheng Liang: funding acquisition, project administration, resources, investigation, supervision, writing – review & editing. Deqian Liu: formal analysis, writing – review & editing. Qianjun Liu: writing – review & editing.

Conflicts of interest

There are no conflicts to declare.

Acknowledgements

This research was funded by financial support provided by the National Natural Science Foundation of China (Grant No. 22008255).

References

1 C. Du, B. Liu, J. Hu and H. Li, Determination of iodine number of activated carbon by the method of ultraviolet-visible spectroscopy, *Mater. Lett.*, 2021, **285**, 129137.
2 S. Hirunpraditkoon, P. Srinophakun, N. Sombun and E. J. Moore, Synthesis of activated carbon from *jatropha* seed coat and application to adsorption of iodine and methylene blue, *Chem. Eng. Commun.*, 2015, **202**(1), 32–47.
3 G. Qu, Y. Han, J. Qi, X. Xing, M. Hou, Y. Sun, X. Wang and G. Sun, Rapid iodine capture from radioactive wastewater by green and low-cost biomass waste derived porous silicon–carbon composite, *RSC Adv.*, 2021, **11**(9), 5268–5275.
4 Ö. Şahin, C. Saka, A. A. Ceyhan and O. Baytar, The pyrolysis process of biomass by two-stage chemical activation with different methodology and iodine adsorption, *Energy Sources, Part A Recovery, Util. Environ. Eff.*, 2016, **38**(12), 1756–1762.
5 X. Long, Y. Chen, Q. Zheng, X. Xie, H. Tang, L. Jiang, J. Jiang and J. Qiu, Removal of iodine from aqueous solution by PVDF/ZIF-8 nanocomposite membranes, *Sep. Purif. Technol.*, 2020, **238**, 116488.
6 Y. Tachibana, M. Nogami, M. Nomura and T. Suzuki, Simultaneous removal of various iodine species in aqueous solutions of high salt concentrations using novel functional adsorbents, *J. Radioanal. Nucl. Chem.*, 2016, **307**(3), 1911–1918.
7 S. Ma and H. Zhou, Gas storage in porous metal–organic frameworks for clean energy applications, *Chem. Commun.*, 2010, **46**(1), 44–53.
8 R. Dawson, A. I. Cooper and D. J. Adams, Nanoporous organic polymer networks, *Prog. Polym. Sci.*, 2012, **37**(4), 530–563.
9 G. Zhu, X. Xing, J. Wang and X. Zhang, Effect of acid and hydrothermal treatments on the dye adsorption properties of biomass-derived activated carbon, *J. Mater. Sci.*, 2017, **52**(13), 7664–7676.
10 D. Liang, Q. Xie, J. Liu, F. Xie, D. Liu and C. Wan, Mechanism of the evolution of pore structure during the preparation of activated carbon from Zhundong high-alkali coal based on gas-solid diffusion and activation reactions, *RSC Adv.*, 2020, **10**(55), 33566–33575.
11 Q. Zhuang, J. Cao, Y. Wu, M. Zhao, X. Zhao, Y. Zhao and H. Bai, Heteroatom nitrogen and oxygen co-doped three-dimensional honeycomb porous carbons for methylene blue efficient removal, *Appl. Surf. Sci.*, 2021, **546**, 149139.
12 C. Zheng, X. Zhou, H. Cao, G. Wang and Z. Liu, Synthesis of porous graphene/activated carbon composite with high packing density and large specific surface area for supercapacitor electrode material, *J. Power Sources*, 2014, **258**, 290–296.
13 K. Zhu, K. Egeblad and C. H. Christensen, Mesoporous Carbon Prepared from Carbohydrate as Hard Template for Hierarchical Zeolites, *Eur. J. Inorg. Chem.*, 2007, **2007**(25), 3955–3960.
14 D. Liang, Q. Xie, C. Wan, G. Li and J. Cao, Evolution of structural and surface chemistry during pyrolysis of Zhundong coal in an entrained-flow bed reactor, *J. Anal. Appl. Pyrolysis*, 2019, **140**, 331–338.
15 Y. Wu, X. Zhao, J. Cao, S. He, Z. Hao, H. Yu, G. Sun and X. Wei, Porous Carbons Derived from Lignite Mixed with Zn^{2+}-Doped Lignin for Electric Double-Layer Capacitor, *Int. J. Electrochem. Sci.*, 2017, **12**(9), 8132–8147.
16 Y. Wu, J. Cao, X. Zhao, Z. Hao, Q. Zhuang, J. Zhu, X. Wang and X. Wei, Preparation of porous carbons by hydrothermal carbonization and KOH activation of lignite and their performance for electric double layer capacitor, *Electrochim. Acta*, 2017, **252**, 397–407.
17 Q. Zhuang, J. Cao, Z. Hao, X. Wan, Y. Wu, Z. Ni, X. Zhao and X. Wei, Oxygen-rich Hierarchical Porous Carbon Derived from Coal Tar Pitch for Superior Electric Double Layer Capacitor Application, *Int. J. Electrochem. Sci.*, 2018, **13**(9), 8440–8453.
18 R. Atchudan, T. N. J. I. Edison, S. Perumal and Y. R. Lee, Green synthesis of nitrogen-doped graphitic carbon sheets with use of *Prunus persica* for supercapacitor applications, *Appl. Surf. Sci.*, 2017, **393**, 276–286.
19 C. Dai, J. Wan, J. Yang, S. Qu, T. Jin, F. Ma and J. Shao, H_3PO_4 solution hydrothermal carbonization combined with KOH activation to prepare argy wormwood-based porous carbon

for high-performance supercapacitors, *Appl. Surf. Sci.*, 2018, **444**, 105–117.

20 M. Demir, Z. Kahveci, B. Aksoy, N. K. R. Palapati, A. Subramanian, H. T. Cullinan, H. M. El-Kaderi, C. T. Harris and R. B. Gupta, Graphitic Biocarbon from Metal-Catalyzed Hydrothermal Carbonization of Lignin, *Ind. Eng. Chem. Res.*, 2015, **54**(43), 10731–10739.

21 J. Deng, T. Xiong, H. Wang, A. Zheng and Y. Wang, Effects of Cellulose, Hemicellulose, and Lignin on the Structure and Morphology of Porous Carbons, *ACS Sustainable Chem. Eng.*, 2016, **4**(7), 3750–3756.

22 S. A. Nicolae, H. Au, P. Modugno, H. Luo, A. E. Szego, M. Qiao, L. Li, W. Yin, H. J. Heeres, N. Berge and M. Titirici, Recent advances in hydrothermal carbonisation: from tailored carbon materials and biochemicals to applications and bioenergy, *Green Chem.*, 2020, **22**(15), 4747–4800.

23 C. Falco, J. P. Marco-Lozar, D. Salinas-Torres, E. Morallón, D. Cazorla-Amorós, M. M. Titirici and D. Lozano-Castelló, Tailoring the porosity of chemically activated hydrothermal carbons: Influence of the precursor and hydrothermal carbonization temperature, *Carbon*, 2013, **62**, 346–355.

24 A. Jain, S. Jayaraman, R. Balasubramanian and M. P. Srinivasan, Hydrothermal pre-treatment for mesoporous carbon synthesis: enhancement of chemical activation, *J. Mater. Chem. A*, 2014, **2**(2), 520–528.

25 M. Li, W. Li and S. Liu, Hydrothermal synthesis, characterization, and KOH activation of carbon spheres from glucose, *Carbohydr. Res.*, 2011, **346**(8), 999–1004.

26 B. Hu, K. Wang, L. Wu, S. H. Yu, M. Antonietti and M. M. Titirici, Engineering Carbon Materials from the Hydrothermal Carbonization Process of Biomass, *Adv. Mater.*, 2010, **22**(7), 813–828.

27 Z. Hao, J. Cao, X. Zhao, Y. Wu, J. Zhu, Y. Dang, Q. Zhuang and X. Wei, Preparation of porous carbon spheres from 2-keto-l-gulonic acid mother liquor by oxidation and activation for electric double-layer capacitor application, *J. Colloid Interface Sci.*, 2018, **513**, 20–27.

28 J. Wu, J. Wang, J. Liu, Y. Yang, J. Cheng, Z. Wang, J. Zhou and K. Cen, Moisture removal mechanism of low-rank coal by hydrothermal dewatering: Physicochemical property analysis and DFT calculation, *Fuel*, 2017, **187**, 242–249.

29 Z. Liu, F. Zhang and J. Wu, Characterization and application of chars produced from pinewood pyrolysis and hydrothermal treatment, *Fuel*, 2010, **89**(2), 510–514.

30 M. Xu, Q. Huang, R. Sun and X. Wang, Simultaneously obtaining fluorescent carbon dots and porous active carbon for supercapacitors from biomass, *RSC Adv.*, 2016, **6**(91), 88674–88682.

31 X. Zhang, C. Zhang, P. Tan, X. Li, Q. Fang and G. Chen, Effects of hydrothermal upgrading on the physicochemical structure and gasification characteristics of Zhundong coal, *Fuel Process. Technol.*, 2018, **172**, 200–208.

32 X. Li, J. Hayashi and C. Li, FT-Raman spectroscopic study of the evolution of char structure during the pyrolysis of a Victorian brown coal, *Fuel*, 2006, **85**(12–13), 1700–1707.

33 Y. Yi, P. Wang, G. Fan, Z. Wang, S. Chen, T. Xue and Y. Wen, Hierarchically Porous Carbon Microsphere Doped with Phosphorus as a High Conductive Electrocatalyst for Oxidase-like Sensors and Supercapacitors, *ACS Sustainable Chem. Eng.*, 2020, **8**(26), 9937–9946.

34 H. Wang, H. Deng, Y. He, L. Huang, D. Wei, T. Hao, S. Wang, L. Jin and L. Zhang, Facile and sustainable synthesis of slit-like microporous N-doped carbon with unexpected electrosorption performance, *Chem. Eng. J.*, 2020, **396**, 125249.

35 Y. Shen and N. Zhang, A facile synthesis of nitrogen-doped porous carbons from lignocellulose and protein wastes for VOCs sorption, *Environ. Res.*, 2020, **189**, 109956.

36 C. Falco, F. Perez Caballero, F. Babonneau, C. Gervais, G. Laurent, M. Titirici and N. Baccile, Hydrothermal Carbon from Biomass: Structural Differences between Hydrothermal and Pyrolyzed Carbons *via* ^{13}C Solid State NMR, *Langmuir*, 2011, **27**(23), 14460–14471.

37 M. Sevilla and R. Mokaya, Energy storage applications of activated carbons: supercapacitors and hydrogen storage, *Energy Environ. Sci.*, 2014, **7**(4), 125–128.

38 C. Qin, S. Wang, Z. Wang, K. Ji, S. Wang, X. Zeng, X. Jiang and G. Liu, Hierarchical porous carbon derived from *Gardenia jasminoides* Ellis flowers for high performance supercapacitor, *J. Energy Storage*, 2021, **33**, 601–610.

39 H. Dong, M. Li, Y. Jin, Y. Wu, C. Huang and J. Yang, Preparation of Graphene-Like Porous Carbons With Enhanced Thermal Conductivities From Lignin Nanoparticles by Combining Hydrothermal Carbonization and Pyrolysis, *Front. Energy Res.*, 2020, **8**, 14801–14810.

40 X. Yu, J. Lu, C. Zhan, R. Lv, Q. Liang, Z. Huang, W. Shen and F. Kang, Synthesis of activated carbon nanospheres with hierarchical porous structure for high volumetric performance supercapacitors, *Electrochim. Acta*, 2015, **182**, 908–916.

41 X. Zhao, Key Laboratory Of Coal Processing And Efficient Utilization Ministry Of Education, C. U. O. M., Preparation and Characterization of Activated Carbons from Oxygen-rich Lignite for Electric Double-layer Capacitor, *Int. J. Electrochem. Sci.*, 2018, 2800–2816.

42 A. Mianowski, M. Owczarek and A. Marecka, Surface Area of Activated Carbon Determined by the Iodine Adsorption Number, *Energy Sources, Part A Recovery, Util. Environ. Eff.*, 2007, **29**(9), 839–850.

43 B. Guo, C. Hou, L. Fan and Z. Sun, Effect of Extraction Temperature on Hyper-coal Structure and Electrochemistry of Coal-Based Activated Carbon, *Chin. J. Inorg. Chem.*, 2018, **34**(9), 1615–1624.

44 X. Zhao, S. Huang, J. Cao, X. Wei, K. Magarisawa and T. Takarada, HyperCoal-derived porous carbons with alkaline hydroxides and carbonate activation for electric double-layer capacitors, *Fuel Process. Technol.*, 2014, **125**, 251–257.